ElasT: a toolkit for thermoelastic calculations

Yunguo Li[1,2,3]*, Lidunka Vočadlo[1], and John P. Brodholt[1,4]

[1]*Department of Earth Sciences, UCL, Gower Street, London, WC1E 6BT, UK*

[2]*CAS Key Laboratory of Crust–Mantle Materials and Environments, School of Earth and Space Sciences, University of Science and Technology of China, Hefei, Anhui 230026, China*

[3]*CAS Center for Excellence in Comparative Planetology, USTC, Hefei, Anhui 230026, China*

[4]*Centre for Earth Evolution and Dynamics, University of Oslo, Oslo, Norway*

[*]Corresponding author: Yunguo Li (email: liyunguo@ustc.edu.cn).

Abstract

A toolkit that simplifies the calculation of solid-state elastic properties at finite temperatures to a one-shot task is developed. We report the improvement and automation of the stress-strain method, which relies on the averaged stresses from *ab initio* or classical calculations. Stresses obtained from strained crystal lattices at zero and finite temperatures can be directly extracted to fit the strain-stress relationship and get the elastic constants. Furthermore, the finite-temperature elastic constants can also be obtained by solving a system of overdetermined linear equations directly under constant pressure dynamics (NPT, NPH, etc.) within the stress-strain method, which does not require the equilibrated lattice as a prior condition. It is shown that the elastic constants converge quickly in constant pressure dynamics. This approach proves to be robust and can significantly reduce computational cost.

Keywords

Thermoelasticity; Elastic constants; Stress-train method; Molecular dynamics

Program Summary

Program Title: ElasT, VERSION 1.1

Licensing provision: GNU General Public License, version 3

Programming language: Fortran

Nature of problem: Calculations of the single-crystal elastic constants at finite temperature conditions.

Solution method: Solve the stress-strain linear equations in constant volume or constant pressure ensembles.

Introduction

Elasticity is an important aspect of any material because it directly links the nature of chemical bonds to fundamental solid-state properties. It is also essential to the understanding of important processes like the propagation of elastic waves and fracture mechanics, and is therefore of wide interest in both materials- and Earth sciences. However, the accurate measurement of elastic constants in the laboratory is still challenging, especially at elevated temperature-pressure conditions. Therefore, a complementary theoretical approach to calculate elastic constants is required.

The developments of density functional theory (DFT) [1] and computation power now enable quantum mechanical calculations of hundreds of atoms that predict accurate ground-state properties. Ground-state elastic constants at zero temperatures can be accurately obtained from DFT calculations by using the energy-strain method, stress–strain approach, and density functional perturbation theory [2]. Finite-temperature elastic properties from DFT need to resort to either the quasi-harmonic approximation (QHA) or *ab initio* molecular dynamics (AIMD). Both methods are computationally demanding: the former involves intensive phonon calculations and the latter needs long-time sampling. Although there are methods to circumvent the intensive phonon calculations [3-5], the QHA method is still limited to some temperatures and will fail at higher temperatures due to the enhanced anharmonic effect [6, 7].

Reliable finite-temperature elastic constants can be derived from AIMD calculations using either the strain-energy approach that analyses the total energies of strained crystal structures, or the stress-strain approach that analyses the stresses resulting from the applied strains [2]. Although the methods are simple and straightforward, the calculation of elastic constants at finite temperature is extremely challenging and computer intensive since converged stresses/energies have to be collected from molecular dynamics (MD) performed on many strained structures for long simulation times [8]. The process required to create strained supercells, collect and analyse the MD data can be cumbersome and time consuming.

Therefore, in this toolkit, we implement the well known stress-strain method that uses as input the averaged stresses of strained supercells from constant-volume MD runs. We also implement a

further stress-strain method that uses a single constant pressure MD run (NPT, NPH, etc.) to calculate the elastic constants, which does not require the equilibrium structure as input and can greatly reduce the computational cost, especially for low-symmetry crystals. The method, implementation, and application are introduced in the following sections.

2 Methods

2.1 Elasticity

Elasticity quantifies deformation in a solid under applied forces. The amount of deformation is known as *strain*, and the applied force per unit area is called *stress* [2].

Consider a pair of points in close proximity at $\boldsymbol{x}$ and $\boldsymbol{x}+\boldsymbol{dx}$ in a solid, which are displaced to locations $\boldsymbol{x}+\boldsymbol{u}(\boldsymbol{x})$ and $\boldsymbol{x}+\boldsymbol{dx}+\boldsymbol{u}(\boldsymbol{x}+\boldsymbol{dx})$ under elastic deformation. Since the displacement is very small, the squared distance between the points after the displacement can be written as a Taylor expansion about the point at $\boldsymbol{x}$

$$\sum_i \left(dx_i + \sum_j \frac{\partial u_i}{\partial x_j} dx_j \right)^2 = \sum_i dx_i^2 + 2 \sum_{i,j} dx_i \frac{\partial u_i}{\partial x_j} dx_j + \sum_{i,j,k} \frac{\partial u_i}{\partial x_j} dx_j \frac{\partial u_i}{\partial x_k} dx_k \qquad (1)$$

where *i*, *j*, and *k* run over the Cartesian components. The change of the squared distance after displacement is given in the last two terms of Eq. 1 and can be rewritten as

$$D(dx) = \sum_{i,j} dx_i \left[\frac{\partial u_i}{\partial x_j} + \frac{\partial u_j}{\partial x_i} + \sum_k \frac{\partial u_k}{\partial x_i} \frac{\partial u_k}{\partial x_j} \right] dx_j = 2 \sum_{i,j} dx_i \, \varepsilon_{ij} dx_j \qquad (2)$$

where ε_{ij} is defined as the component of the strain tensor. Neglecting the trivial second-order term, this can be approximated as

$$\varepsilon_{ij} = \frac{1}{2} \left(\frac{\partial u_i}{\partial x_j} + \frac{\partial u_j}{\partial x_i} \right) \qquad (3)$$

and the Green-Lagrange full strain tensor is

$$\varepsilon = \begin{pmatrix} \varepsilon_{xx} & \varepsilon_{xy} & \varepsilon_{xz} \\ \varepsilon_{yx} & \varepsilon_{yy} & \varepsilon_{yz} \\ \varepsilon_{zx} & \varepsilon_{zy} & \varepsilon_{zz} \end{pmatrix} \qquad (4)$$

Let us take a small area $\boldsymbol{\Delta A_i}$ in the solid that is orthogonal to the $\boldsymbol{i}$-direction. Assume the sum of the applied forces in the solid is zero (otherwise we would have translation). The total force acting on the small area can be written as

$$\Delta \boldsymbol{F} = \sum_i \Delta F_i \cdot \boldsymbol{i} \qquad (5)$$

Then the stresses can be defined as

$$\sigma_{ij} = \lim_{\Delta A_i \to 0} \frac{\Delta F_j}{\Delta A_i} \tag{6}$$

where *i* and *j* refer to the plane and force directions, respectively. Written in matrix form, the stress tensor is given by

$$\sigma = \begin{pmatrix} \sigma_{xx} & \sigma_{xy} & \sigma_{xz} \\ \sigma_{yx} & \sigma_{yy} & \sigma_{yz} \\ \sigma_{zx} & \sigma_{zy} & \sigma_{zz} \end{pmatrix} \tag{7}$$

Within the harmonic limit, the relationship between the strain and stress is linear and written as

$$\sigma_{ij} = C_{ijkl}\varepsilon_{kl} \tag{8}$$

where C_{ijkl} is a component of the fourth-order elastic stiffness tensor (elastic constant) and in total there are 81 components. In the static equilibrium state, $\sigma_{ij} = \sigma_{ji}$ and $\varepsilon_{ij} = \varepsilon_{ji}$. So, both σ and ε can be contracted to a six-component tensor. The number of independent elastic stiffness constants is reduced to 21. In the Voigt notation [9], Eq. 8 can be rewritten in matrix form as

$$\begin{pmatrix} \sigma_1 \\ \sigma_2 \\ \sigma_3 \\ \sigma_4 \\ \sigma_5 \\ \sigma_6 \end{pmatrix} = \begin{pmatrix} C_{11} & C_{12} & C_{13} & C_{14} & C_{15} & C_{16} \\ C_{21} & C_{22} & C_{23} & C_{24} & C_{25} & C_{26} \\ C_{31} & C_{32} & C_{33} & C_{34} & C_{35} & C_{36} \\ C_{41} & C_{42} & C_{43} & C_{44} & C_{45} & C_{46} \\ C_{51} & C_{52} & C_{53} & C_{54} & C_{55} & C_{56} \\ C_{61} & C_{62} & C_{63} & C_{64} & C_{65} & C_{66} \end{pmatrix} \begin{pmatrix} \varepsilon_1 \\ \varepsilon_2 \\ \varepsilon_3 \\ \varepsilon_4 \\ \varepsilon_5 \\ \varepsilon_6 \end{pmatrix} \tag{9}$$

2.2 Stress-strain method

In the stress-strain method, a number of strains are applied to the crystal lattice and the induced stresses can be calculated from *ab initio* or classical methods, and the elastic constants can be obtained through Eq. 9. The number of distinct elastic constants further reduces according to crystal symmetry, and this reduces the number of strains and stresses that need to be calculated. The patterns of elastic constants for different lattice types are shown in Fig. 1.

To reduce computational cost, the number of selected strains should be as few as possible. However, the use of small strains will bring in large uncertainty, while the use of large strains will invalidate the strain-stress linearity. To overcome this, several strains, including both positive and negative strains, should be used and the elastic constants corresponding to the equilibrium state can be obtained from fitting the stress-strain relationship and finding the slope at zero strain. For finite-temperature calculations (NVT), stresses are averaged over the simulation time, but this can

be very computer intensive, especially for low symmetry crystals or alloys. For example, a monoclinic crystal needs at least four different strains to solve Eq. 9. If we take four magnitudes per strain (two either side of equilibrium) to obtain a polynomial fit, then there are 17 (16 plus one NPT run for relaxation) MD calculations in total to be performed.

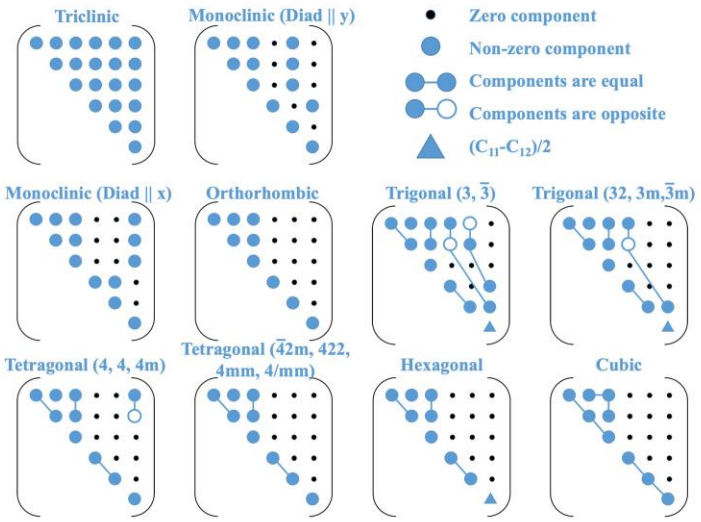

Figure 1. The patterns of elastic stiffness tensor for different types of lattice [10].

2.3 Stress-strain method in constant pressure ensembles

We note Parrinello and Rahman [11] first presented the strain fluctuation formula that enables the derivation of elastic constants from constant pressure ensembles

$$C_{ijkl} = \frac{k_B T}{\langle V \rangle}\left[\langle \varepsilon_{ij}\varepsilon_{kl}\rangle - \langle \varepsilon_{ij}\rangle\langle \varepsilon_{kl}\rangle\right]^{-1} \quad (10)$$

where k_B is the Boltzmann constant and T the temperature. But it converges very slowly with inefficient strain fluctuation. Gusev et al. [12] improved the convergence by making use of the stress fluctuation

$$C_{ijkl} = \langle \varepsilon_{ij}\sigma_{mn}\rangle\langle \varepsilon_{mn}\varepsilon_{kl}\rangle^{-1} \quad (11)$$

It is important to note that the methods assume the validity of linear elasticity. For soft materials the strain could be large and exceed the linear region, and thus lead to some underestimation of the elastic constants. Buffering the simulation material with an elastic bath can remedy this [13, 14], however it would require modification of the particular molecular dynamics code used. Here we propose another strategy. The amplitude of strain fluctuation in an NPT ensemble is a function

of bulk modulus B_T and system volume [15], expressed as $\sqrt{\frac{k_B T}{B_T \langle V \rangle}}$. Therefore, the strain fluctuation will be reduced by increasing the supercell in an MD run, and the problem of strain-stress nonlinearity can be avoided without resorting to complicated methods. Since our aim is to provide easy transferability to any MD code and for more general purpose and usage, we follow the idea of Gusev *et al*. (1996) and recommend users to resort to bigger supercells for soft materials. Typically, the supercell should be large enough so that the strain fluctuation is no more than 3%, but this also depends on materials under investigation.

In constant pressure dynamics, e.g., NPT dynamics, the lattice tensor *R* fluctuates around its equilibrium states $\bar{R}$. The Green-Lagrange strain tensor at each MD step can be calculated

$$\varepsilon = \bar{R}^{-1} \cdot R - I \tag{12}$$

where *I* is the identity tensor. The corresponding stresses can be calculated in NPT dynamics by differentiating the total energy with respect to the lattice vectors. The linear relationship in Eq. 9 becomes

$$\begin{pmatrix} \sigma_1 \\ \sigma_2 \\ \sigma_3 \\ \sigma_4 \\ \sigma_5 \\ \sigma_6 \end{pmatrix} = \begin{pmatrix} \overbrace{\begin{matrix} \varepsilon_1 & \varepsilon_2 & \cdot & \cdot & \cdot & 0 \\ 0 & \varepsilon_1 & \cdot & \cdot & \cdot & 0 \\ 0 & 0 & \cdot & \cdot & \cdot & 0 \\ 0 & 0 & \cdot & \cdot & \cdot & 0 \\ 0 & 0 & \cdot & \cdot & \cdot & 0 \\ 0 & 0 & \cdot & \cdot & \cdot & \varepsilon_6 \end{matrix}}^{21 \text{ columns}} \end{pmatrix} \begin{pmatrix} C_{11} \\ C_{12} \\ \cdot \\ \cdot \\ \cdot \\ C_{66} \end{pmatrix} \tag{13}$$

For elastic calculations under high pressure, the stress tensor σ above should be subtracted from the hydrostatic pressure. The linear equations with 21 unknown variables (C_{ij}) can be solved with a sufficient number of MD runs, and the results should converge as the number of MD steps increases. Therefore, the elastic constants can be obtained directly from one NPT dynamics run. For monoclinic crystals, this reduces the computational cost by over 90%.

3 Implementation

The calculation of elastic constants using stress-strain methods described above can be tedious and so we have automated the methods (under both the constant-volume and constant-pressure dynamics) into a toolkit named ElasT, which simplifies such calculations to a single stage task. We implement both methods – a) the widely used stress-strain method under constant-volume dynamics and b) the more efficient stress-strain method under constant-pressure dynamics.

In constant-volume dynamics, stresses are collected from strained calculations, and the elastic constants are obtained by polynomial fitting of the stress-strain relationship. First, the lattice parameters obtained from the NPT simulation are needed to create a unit cell to which strains are applied. The stresses on the strained cells can then be obtained from NVT simulations at the target temperature.

The more efficient stress-strain method under constant pressure NPT dynamics is also implemented. It collects the stress and strain tensors in each MD step and calculates the elastic constants from solving a system of overdetermined linear equations. Only the isothermal elastic constants can be correctly derived from the NPT simulations. In NPT simulations, the strain or volume oscillate with a frequency determined by the fictious mass of the lattice. If the frequency is much larger than the temperature oscillation, the system is assumed to be adiabatic and the derived elastic constants should, therefore, also be adiabatic. However, fast volume oscillation can perturb the trajectory and lead to energy deviations, which make the derived adiabatic elastic constants incorrect. Conversely, infinitely slow strain oscillation turns the constant pressure dynamics into constant volume, and no strains can be used to derive the elastic constants. Therefore, in order to get the correct isothermal elastic constants from an NPT simulation, a suitable barostat mass should be used and the temperature oscillation must be much faster than the strain fluctuation.

At present, the toolkit is only interfaced to the VASP code [16], but it can be easily extended to other codes like Quantum Espresso [17], or to classical calculations, by converting stresses and trajectories from other codes to the VASP format. The implementation assumes that the crystal structures are in their standard orientations. Together with the elastic stiffness and compliance tensors, aggregate properties using different averaging methods (Reuss, Voigt and Voigt–Reuss–Hill) [9] are also calculated.

Test calculations were performed to validate the implementation and can be found at the National Geoscience Data Centre (NGDC) [18]. The structure relaxations and total energy calculations were performed using the VASP code based on DFT [16], applying the projector augmented wave (PAW) potentials [19]. Exchange-correlation was treated by the generalized gradient approximation (GGA) [20]. The plane-wave cutoff energy was taken as 1.5 times of the maximum cutoff defined in the PAW potential. The k-mesh for the Brillouin zone sampling was

tested to converge the total energies to 5 meV/atom. The residual forces and stresses were relaxed to be less than 0.002 eV/Å and 0.1 GPa, respectively. For MD runs, we employed the Souza-Martins barostat and Nosé–Poincaré thermostat implemented in VASP by Hernández [21]; a timestep of 1 *fs* was used for both NPT and NVT.

4 Application and discussion

The stress-strain methods described above have been successfully applied to crystals of different materials and lattice types. The strains used and implemented in this toolkit are listed in Table 1. Four degrees of strain, namely, ± 0.02 and ± 0.01, were applied to each type of strain. The elastic constants corresponding to the unstrained equilibrium states were then calculated from second-order polynomial fitting.

Table 2 tabulates the calculated elastic stiffness constants and aggregate properties in comparison with the available experimental or theoretical data at 0 K. Fig. 2 plots the calculated elastic constants against the data from other studies. Overall, the calculated elastic constants are very close to those of experiments or other calculations. The examined crystals include the metallic, semiconducting, and insulating elements/compounds. Monoclinic AlCu (space group *I*12/*m*1) is an intermetallic phase and its elastic properties affect the overall mechanical properties of the widely used Al-Cu alloys [22]. The experimental measurement of its elastic constants is not available. The calculated elastic properties by the toolkit, especially the aggregate properties, match well with the other theoretical calculations. $TiSi_2$ takes an orthorhombic lattice with the space group of *Fddd*. The calculated elastic properties agree well with the experiment data [23]. α-Al_2O_3 (space group *R*-3*c*) is an insulator with a trigonal lattice. Although the calculated elastic constants of α-Al_2O_3 are close to the experimental values [24], they are consistently smaller. Because the electrons in α-Al_2O_3 are more localized than in metals, GGA usually overestimates the lattice constants and underestimates the elastic constants. β-Sn (space group *I*4/*mmm*) in the tetragonal lattice is a semiconductor. The calculated elastic constants also match well with the experimental data [25] except for C_{12}, for which the calculated value is 56 GPa while the experimental value is 23 GPa. However, another experiment gave C_{12} as 49 GPa [26]. The calculated elastic properties of hexagonal Mg and cubic Si also match well with the experimental data [27, 28]. Note that, although agreement is not perfect between DFT and experimental data in some places, it may be due to the use of the same setting for metals, semiconductors and insulators;

since we are only interested in the implementation of the method here, we do not discuss further the accuracy of DFT results.

Table 1. The list of applied strains for the seven types of crystal lattice used in the toolkit. Δ designates the applied strain.

Strain Tensor	Crystal Lattice																			
	Triclinic						Monoclinic				Orthorhombic		Trigonal		Tetragonal		Hexagonal		Cubic	
ε_1	Δ	0	0	0	0	0	Δ	0	0	0	Δ/2	-Δ/2	0	0	0	Δ	0	Δ	0	Δ
ε_2	0	Δ	0	0	0	0	0	Δ	0	0	Δ/2	Δ/2	0	Δ	0	Δ	Δ/2	0	0	0
ε_3	0	0	Δ	0	0	0	0	0	0	Δ	0	0	Δ	0	Δ	0	Δ	0	Δ	0
ε_4	0	0	0	Δ	0	0	Δ	0	0	0	Δ	0	0	Δ	0	0	Δ	Δ	0	0
ε_5	0	0	0	0	Δ	0	0	0	Δ	0	0	Δ	0	0	0	0	0	0	0	0
ε_6	0	0	0	0	0	Δ	0	Δ	0	0	0	0	Δ	0	Δ	Δ	0	0	0	Δ

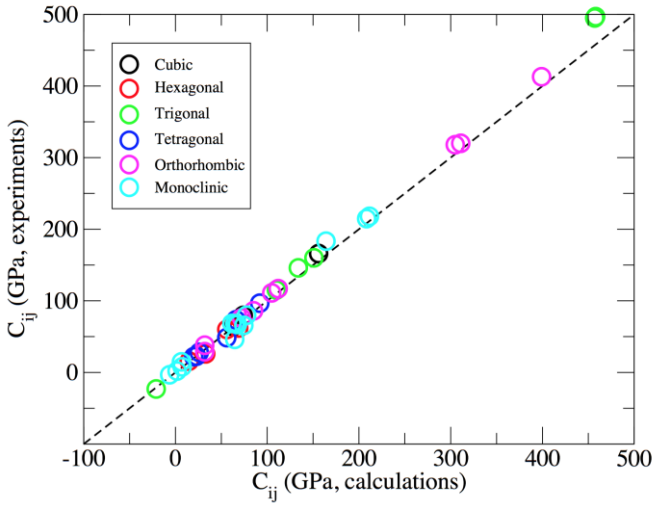

Figure 2. Plot of elastic stiffness constants calculated by the toolkit against other experimental/theoretical data in Table 2.

Table 2. List of elastic stiffness constants and aggregate properties calculated by the toolkit in comparison with other experimental or theoretical data. Only independent elastic constants are shown. Aggregate properties (B: bulk modulus, G: shear modulus, E: Young's modulus, and γ: Poisson's ratio) are only given in the Voigt average.

C_{ij}	Monoclinic AlCu		Orthorhombic TiS_2		Trigonal Al_2O_3		Tetragonal Sn		Hexagonal Mg		Cubic Si	
	DFT	DFT [11]	DFT	Exp. [12]	DFT	Exp. [13]	DFT	Exp. [14]	DFT	Exp. [16]	DFT	Exp. [17]
C_{11}	208	215	305	318	457	495	66	73	56	60	156	166
C_{22}	211	218	311	320								

C_{33}	164	183	399	413	458	497	92	87	69	62		
C_{44}	62	69	105	111	134	146	20	22	15	16	74	80
C_{55}	65	46	72	76								
C_{66}	78	80	112	117			23	23				
C_{12}	68	67	32	29	151	160	56	23	33	26	63	64
C_{13}	75	66	32	38	110	115	26	28	20	22		
C_{14}					-21	-23						
C_{15}	7.4	7.9										
C_{23}	65	68	85	86								
C_{25}	-6	-3										
C_{35}	7	15										
C_{46}	2	2										
B	111	113	146	149	235	252	48	58	36	—	94	98
G	66	67	117	121	151	163	20	18	15	—	63	—
E	165	167	274	278	372	—	52	50	40	—	155	—
γ	0.252	0.25	0.186	0.188	0.236	—	0.318	0.36	0.315	—	0.225	—

For finite-temperature elastic calculations, we tested our Toolkit on cubic Si. The stress-strain method implemented under constant pressure dynamics within our Toolkit directly provides the elastic properties from a single MD run, while the widely used stress-strain method needs the relaxed lattice from NPT dynamics and the averaged stresses from the subsequent NVT dynamics on strained cells.

The isothermal elastic constants C_{ij}^T of cubic Si were calculated by the two methods at 300 K, 600 K, 900 K and 1200 K. Adiabatic elastic constants C_{ij}^S can be obtained via the relationship [29]

$$C_{ij}^S = C_{ij}^T + \frac{TV(T)\lambda_i(T)\lambda_j(T)}{C_V(T)} \qquad (14)$$

where $C_V(T)$ is the molar constant-volume specific heat of the system, $V(T)$ is the molar volume of the system, and

$$\lambda_i(T) = -\sum_j \alpha_j(T) C_{ij}^T(T) \qquad (15)$$

$\alpha_j(T)$ is the linear thermal expansion coefficient. However, since the thermal expansion is small for silicon, the corrections to adiabatic elastic constants are less than 1 GPa. Therefore, we only give the calculated isothermal elastic constants in comparison with the experimental data in both Table 3 and Fig. 3. The NPT and NVT data are in good agreement, especially for aggregate

properties. The calculated elastic moduli also generally agree with the experimental data but show a deviation of ~10%; this can be significantly improved by using hybrid functionals [30]. As shown in Table 3, C_{11} and B calculated from NPT are generally smaller than the NVT data. Possibly this is due to the fact that the strain in NPT exceeds the region where the stress-strain linearity is valid, since we used a supercell of only 64 atoms. Mg is much softer than Si, and to achieve similar accuracy a bigger supercell must be used. We used a supercell of 144 atoms for hexagonal Mg to calculate its elastic moduli at 600 K, and the results are shown in Table 4. The absolute differences between NPT and NVT results are no larger than those for Si though Mg is much softer. This re-emphasises the need to choose big supercells when calculating elastic constants of soft materials with the NPT method.

The convergence of elastic constants calculated within the NPT dynamics Toolkit are plotted in Fig. 4. The elastic constants quickly approach their converged values after 2 ps. After that, the fluctuations are small and excellent convergence can be achieved after 7 ps.

Table 3. Calculated elastic stiffness constants for the cubic Si at 300 K from NPT and NVT, in comparison with experimental data. Aggregate properties are only given in the Voigt average.

T (K)	P (bar)	Method	Elastic modulus (GPa)					
			C_{11}	C_{12}	C_{44}	B	G	γ
293	1	Exp. [31]	160	59	80	93	68	0.206
300	0	NVT	152	62	72	92	61	0.228
300	0	NPT	146	64	76	91	62	0.221
600	0	NVT	143	61	67	88	56	0.237
600	0	NPT	140	59	69	86	58	0.225
900	0	NVT	135	59	63	84	53	0.240
900	0	NPT	136	59	62	85	52	0.244
1200	0	NVT	132	59	59	83	50	0.249
1200	0	NPT	123	61	60	81	49	0.251

Table 4. Calculated isothermal elastic stiffness constants for the hexagonal Mg at 600 K from NPT and NVT. Aggregate properties are only given in the Voigt average.

T (K)	P (bar)	Method	Elastic modulus (GPa)							
			C_{11}	C_{33}	C_{12}	C_{13}	C_{44}	B	G	γ
600	0	NPT	48	47	14	18	12	27	13	0.293
600	0	NVT	43	51	19	14	15	26	14	0.267

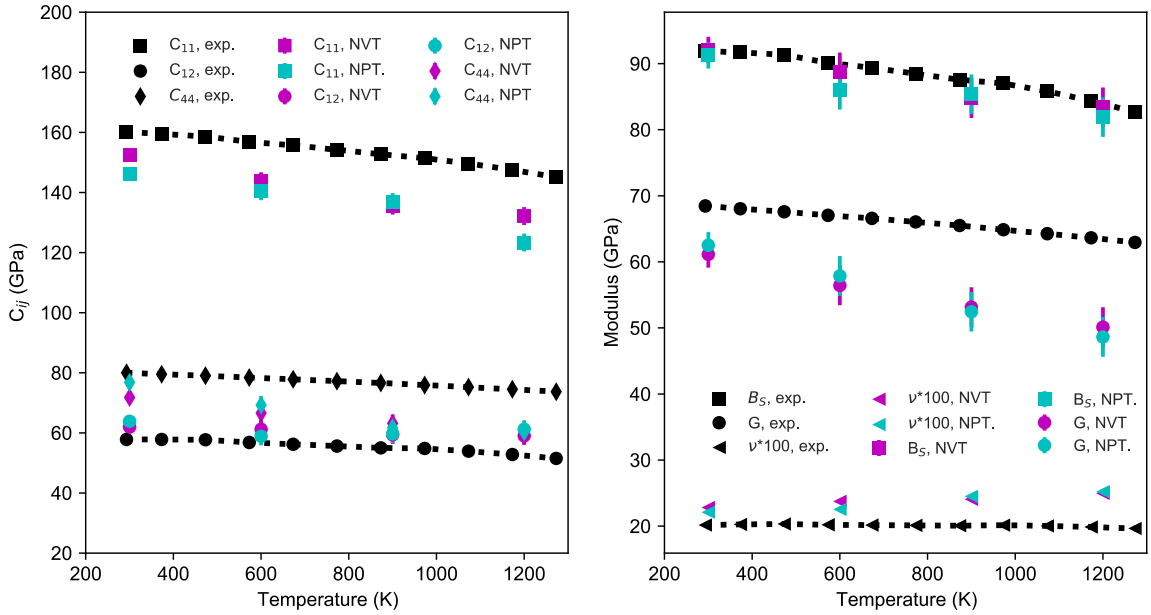

Figure 3. Calculated elastic properties of Si from both NVT and NPT ensembles in comparison with experimental data [31].

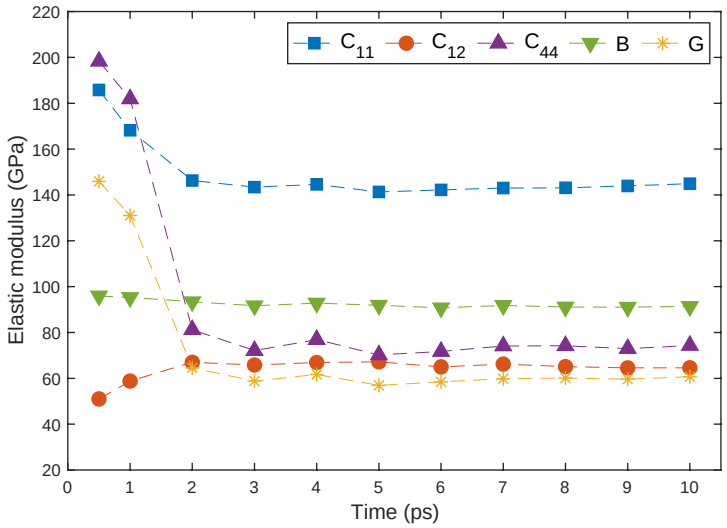

Figure 4. Convergence of the elastic constants of cubic Si with the increasing simulation time in the NPT dynamics. Data at each point were derived from Eq. 11 using all MD steps up to the given time point.

5 Summary

We have automated the stress-strain method to derive elastic constants from *ab initio* calculations. We found the stress-strain method implemented under our constant pressure

dynamics Toolkit can provide almost identical results to the implementation under constant volume dynamics. The computational load is greatly reduced under constant pressure dynamics while remaining sufficiently accurate. This Toolkit will prove invaluable to those carrying out materials and mineral physics research, where thermoelastic properties are frequently sought.

Acknowledgement

Y. Li thank the support from CAS Hundred Talents Program. We acknowledge the support from NERC grant NE/M000125/1. Computation was performed at the ARCHER supercomputer facility. The authors declare no conflicts of interest. This research was also supported by the advanced computing resources provided by the Supercomputing Center of the USTC.

Reference

[1] W. Kohn, L.J. Sham, Self-Consistent Equations Including Exchange and Correlation Effects, Phys. Rev., 140 (1965) A1133--A1138.
[2] M. Born, K. Huang, Dynamical Theory of Crystal Lattices, Clarendon Press1988.
[3] C. Luo, X. Deng, W. Wang, G. Shukla, Z. Wu, R.M. Wentzcovitch, cij: A Python code for quasiharmonic thermoelasticity, Computer Physics Communications, 267 (2021) 108067.
[4] M. Liao, Y. Liu, Z. Lai, J. Zhu, Pressure and temperature dependence of second-order elastic constants from third-order elastic constants in TMC (TM=Nb, Ti, V, Zr), Ceramics International, 47 (2021) 27535-27544.
[5] T. Shao, B. Wen, R. Melnik, S. Yao, Y. Kawazoe, Y. Tian, Temperature dependent elastic constants for crystals with arbitrary symmetry: Combined first principles and continuum elasticity theory, Journal of Applied Physics, 111 (2012) 083525.
[6] J. Bouchet, F. Bottin, Thermal evolution of vibrational properties of $\ensuremath{\alpha}$-U, Physical Review B, 92 (2015) 174108.
[7] Z.-L. Liu, R. Li, X.-L. Zhang, N. Qu, L.-C. Cai, Direct anharmonic correction method by molecular dynamics, Computer Physics Communications, 213 (2017) 122-129.
[8] Y. Li, L. Vočadlo, J. Brodholt, The elastic properties of *hcp*-Fe alloys under the conditions of the Earth's inner core, Earth and Planetary Science Letters, 493 (2018) 118-127.
[9] G. Simmons, H. Wang, others, Single crystal elastic constants and calculated aggregate properties: A Handbook, Mass., MIt Press1971.
[10] J.F. Nye, Physical properties of crystals: their representation by tensors and matrices, Oxford university press1985.
[11] M. Parrinello, A. Rahman, Strain fluctuations and elastic constants, The Journal of Chemical Physics, 76 (1982) 2662-2666.
[12] A.A. Gusev, M.M. Zehnder, U.W. Suter, Fluctuation formula for elastic constants, Physical Review B, 54 (1996) 1-4.
[13] Z. Cui, Y. Sun, J. Li, J. Qu, Combination method for the calculation of elastic constants, Physical Review B, 75 (2007) 214101.
[14] J. Li, Y. Sun, Z. Cui, F. Zeng, Least square method for the calculation of elastic constants, Computer Physics Communications, 182 (2011) 1447-1451.
[15] L. Landau, E. Lifshitz, Statistical Physics, Addison-Wesley, Reading, Mass1958.

[16] G. Kresse, J. Furthmüller, Efficient iterative schemes for ab initio total-energy calculations using a plane-wave basis set, Physical Review B, 54 (1996) 11169-11169.
[17] P. Giannozzi, S. Baroni, N. Bonini, M. Calandra, R. Car, C. Cavazzoni, D. Ceresoli, G.L. Chiarotti, M. Cococcioni, I. Dabo, A. Dal Corso, S. de Gironcoli, S. Fabris, G. Fratesi, R. Gebauer, U. Gerstmann, C. Gougoussis, A. Kokalj, M. Lazzeri, L. Martin-Samos, N. Marzari, F. Mauri, R. Mazzarello, S. Paolini, A. Pasquarello, L. Paulatto, C. Sbraccia, S. Scandolo, G. Sclauzero, A.P. Seitsonen, A. Smogunov, P. Umari, R.M. Wentzcovitch, QUANTUM ESPRESSO: a modular and open-source software project for quantum simulations of materials, Journal of Physics: Condensed Matter, 21 (2009) 395502.
[18] Y. Li, Example Elastic Calculations for ElasT Toolkit, NERC EDS National Geoscience Data Centre, 2021.
[19] P.E. Blöchl, Projector augmented-wave method, Physical Review B, 50 (1994) 17953-17953.
[20] J.P. Perdew, A. Ruzsinszky, G.I. Csonka, O.A. Vydrov, G.E. Scuseria, L.A. Constantin, X. Zhou, K. Burke, Restoring the density-gradient expansion for exchange in solids and surfaces, Physical Review Letters, 100 (2008) 136406-136406.
[21] E. Hernández, Metric-tensor flexible-cell algorithm for isothermal--isobaric molecular dynamics simulations, Journal of Chemical Physics, 115 (2001) 10282-10290.
[22] W. Zhou, L. Liu, B. Li, Q. Song, P. Wu, Structural, elastic, and electronic properties of Al-Cu intermetallics from first-principles calculations, Journal of Electronic Materials, 38 (2009) 356-364.
[23] M. Nakamura, Elastic constants of some transition- metal- disilicide single crystals, Metallurgical and Materials Transactions A, 25 (1994) 331-340.
[24] H. Yao, L. Ouyang, W.Y. Ching, Ab initio calculation of elastic constants of ceramic crystals, Journal of the American Ceramic Society, 90 (2007) 3194-3204.
[25] W.P. Mason, H.E. Bömmel, Ultrasonic Attenuation at Low Temperatures for Metals in the Normal and Superconducting States, The Journal of the Acoustical Society of America, 28 (1956) 930-943.
[26] P.W. Bridgman, Some Properties of Single Metal Crystals, Proc Natl Acad Sci U S A, 10 (1924) 411-415.
[27] T.R. Long, C.S. Smith, Single-crystal elastic constants of magnesium and magnesium alloys, Acta Metallurgica, 5 (1957) 200-207.
[28] H.J. McSkimin, Measurement of Elastic Constants at Low Temperatures by Means of Ultrasonic Waves–Data for Silicon and Germanium Single Crystals, and for Fused Silica, Journal of Applied Physics, 24 (1953) 988-997.
[29] G.F. Davies, Effective elastic moduli under hydrostatic stress—I. quasi-harmonic theory, Journal of Physics and Chemistry of Solids, 35 (1974) 1513-1520.
[30] M. Råsander, M.A. Moram, On the accuracy of commonly used density functional approximations in determining the elastic constants of insulators and semiconductors, The Journal of Chemical Physics, 143 (2015) 144104.
[31] L. Börnstein, Silicon (Si) elastic moduli of Si-I, in: O. Madelung, U. Rössler, M. Schulz (Eds.) Group IV Elements, IV-IV and III-V Compounds, Springer-Verlag Berlin Heidelberg2001.